

The structure of dust aggregates in hierarchical coagulation

C. Dominik¹, D. Paszun, & H. Borel ^{*}

¹Anton Pannekoek Institute for Astronomy, Science Park 904, NL-1098 XH Amsterdam, The Netherlands; E-mail: dominik@uva.nl

DRAFT, November 2, 2016

ABSTRACT

Dust coagulation in interstellar space and protoplanetary disks is usually treated as one of 2 extreme cases: *Particle-Cluster Aggregation* and *Cluster-Cluster Aggregation*. In this paper we study the process of *hierarchical growth*, where aggregates are built from significantly smaller aggregates (but *not* monomers). We show that this process can be understood as a modified, PCA-like process that produces porous, but non-fractal particles whose filling factor is chiefly determined by the porosity of the building blocks. We also show that in a coagulation environment where relative velocities are driven by turbulence, a logarithmically flat mass distribution (equal mass per mass decade) as it is typically found in environments where fragmentation replenishes small grains, leads to a situation where small particles and aggregates dominate the growth of large ones. Therefore, in such environments, hierarchical growth should be seen as the norm. Consequently, we predict that the aggregates in such environments are not fractals with extremely low densities as they would result from extrapolation fractal laws to large sizes. The compactification of aggregates does not only result from collisions with enough energy to restructure aggregates - it starts already earlier by filling voids in particles with smaller grains that contribute to the growth.

interstellar matter – stars: formation – dust: processes

1. Introduction

The formation of planets proceeds in disks surrounding young stars. Small dust grains collide and stick to each other growing to larger and larger sizes. This growth initially involves energies that are insufficient to break or even deform aggregates (also referred to as particles or agglomerates) made of smaller constituents - monomers (also referred to as grains). In the commonly accepted scenario, dust grows to relatively large, at least dm-sized particles. At these sizes aggregates suffer from a very strong head wind (due to sub-Keplerian motion of the gas) that leads to strong radial drift (Weidenschilling 1977) and destructive collisions (e.g. Brauer et al. 2008). These processes are critical to our understanding of planet formation, and they depend strongly on the porosity of the dust grains (Brauer et al. 2007).

The growth of aggregates from small monomers is usually treated in one of two limiting cases: Particle-Cluster Aggregation (PCA) and Cluster-Cluster Aggrega-

tion (CCA). These terms are sometimes used loosely. PCA means the formation of an aggregate by a succession of collisions with individual monomers. Each collision can be seen as an independent collision, the impactors always come in as individual particles and do not collide with other impactors on the way in. CCA means the build-up of a large aggregate in a sequence of collisions of aggregates of similar sizes. In its purest form, the two colliding aggregates will always have exactly the same size, in reality they will be similar in size.

It has been shown that the structure of the aggregates formed by PCA and by CCA, respectively, is very different.

PCA aggregates get a homogeneous structure. The core of the aggregate has a constant density and is therefore not fractal in nature. In full generality this has been shown by Ball & Witten (1984) who demonstrated that the PCA buildup is subject to a causality condition that requires a lower limit for the fractal dimension D_f of the forming aggregate given by $D_f \geq D_{\text{space}} - D_{\text{approach}} + 1$ where D_{space} is the dimension of space and D_{approach} is the fractal dimension of the trajectory of the approaching particle. For ballistic approach trajectories, we have $D_{\text{approach}} = 1$, and in normal 3D space, this means that $D_f \geq 3$. Therefore, pure PCA aggregates are non-fractal.

The case of CCA aggregates has been studied in the laboratory (e.g. Krause & Blum 2004) and theoretically (Kempf et al. 1999; Paszun & Dominik 2006) as well, and it has been shown that such growth leads to much smaller fractal dimensions. The details depend again on the structure of the collision trajectory of the particles and on the rotational state of the colliding aggregates.

Physically, PCA and CCA aggregation represent very different growth conditions. PCA corresponds to a runaway growth situation, where one or a small number of particles consume all the other particles before they have time to aggregate themselves. This means that the typical timescale

^{*} This paper was originally submitted to A&A in June 2009. Despite a positive report by an anonymous referee, it was never published since the referee asked for an analytical derivation of some of the results. D. Paszun had left astronomy by then, so we never did comply with this request, even though it should be possible to do that derivation. I (C. Dominik) am putting it up on arXiv now because the results have renewed relevance in relation to Rosetta results (Bentley et al. 2016), and the various studies on pebble collapse as a model for comet and planetesimal formation (e.g. Lorek et al. 2016; Blum et al. 2014). This study was part of the PhD thesis of Dr. D. Paszun at the University of Amsterdam. An electronic version of that PhD thesis is available at <http://www.astro.uva.nl/static/research/theses/phd/dm-paszun.pdf>

[theses/phd/dm-paszun.pdf](http://www.astro.uva.nl/static/research/theses/phd/dm-paszun.pdf)

for a particle to collide with the runaway aggregate must be shorter than the time to collide with any monomer in the environment. At least in a situation where the aggregation process starts with only small particles present, this is a very unrealistic situation. Therefore, in practice, at least initially CCA is the much more likely situation. A good example is the growth of aggregates under conditions where relative motions are governed by thermal motions, e.g. Brownian motion of particles in a rarefied gas. Such growth has recently been studied under microgravity conditions and indeed it was shown that this process leads to a narrow size distribution (Krause & Blum 2004), implying that the typical collision takes place between two aggregates of similar size. Consequently and as expected, such experiments show the buildup of fractal aggregates, with fractal dimensions around 1.5. As long as the collision velocities are largest between the smallest grains, the growth process will deplete the smallest particles by collisions with other small particles and in this way keep the size distribution narrow. CCA-like growth is the result and will continue until the basic physics of the growth process change. The fractal structure of the aggregates is not even a requirement for growth to proceed in a CCA-like way. As long as small particles are removed efficiently, the size distribution will remain compact and collisions of similar-sized particles will be dominant in determining the growth process.

There are two basic conditions under which the growth process will leave the CCA path and we will call these conditions the *runaway* and the *fragmentation* case.

In the runaway case, the conditions change to those also needed for PCA growth: the relative motions of particles become such that indeed the most likely collision for a small particle or aggregate is the collision with a large particle. In protoplanetary disks, such conditions may arise when systematic motions start to govern the relative motions rather than thermal motions. For example, under the conditions of turbulent motions in the gas, we can have two kinds of particles. Small particles that are very well coupled to the gas follow a similar motion and thus their relative velocities remain small (Voelk et al. 1980; Weidenschilling & Cuzzi 1993; Ormel & Cuzzi 2007). The dust-gas interaction is quantified by the Stokes number $St = \tau_f/\tau_L$, where τ_f is the stopping or friction time of a particle and τ_L is the overturn time of the largest eddies (usually assumed to be of the order of the Kepler time $\sim \Omega^{-1}$). The stopping time of a particle is given by

$$\tau_f = \frac{3}{4c_s} \frac{m}{\rho_g \sigma}, \quad (1)$$

where c_s is the sound speed in the gas, ρ_g is density of gas, m is the mass of a dust particle, and σ is the projected surface of the particle. Larger particles with Stokes numbers close to unity will start to decouple from the gas and find themselves in a sand-blasting stream of gas containing small, well-coupled particles.

The second case is that of *fragmentation*. It was shown by Dullemond & Dominik (2005); Dominik & Dullemond (2008) that the observed abundance of small grains in protoplanetary disks is actually best explained by ongoing fragmentation that destroys aggregates of a certain size and puts the mass of these back into small grains. In such a case, small grains will always contribute to the growth and in this way introduce a hierarchical growth component.

In order to understand the evolution of porosity during the coagulation of dust particles, it is therefore important to understand the effects of hierarchical growth. In this paper, we will study hierarchical growth and describe the structure of aggregates formed in this way.

2. Methods

To study the structure of aggregates resulting from hierarchical growth, we use the model developed by Paszun & Dominik (2006). In this approach, aggregates are treated as rigid bodies that freely move and rotate in 3-dimensional space. Aggregates can move simply ballistically on trajectories that lead to collisions, or they may be embedded in a medium causing both motion and rotation to change frequently (after one stopping length) in order to model Brownian motion. In this study we will concentrate on the low density limit in which the mean Brownian path length of an aggregate is larger than the size of the aggregate, so that the motion can be seen as ballistic during the collision. Paszun & Dominik (2006) had shown that under high density conditions in the innermost parts of the solar nebula this condition may not hold (e.g., aggregates made of 10^3 micron-sized monomers at densities above $\rho_g > 10^{-9}$ g/cm³ have a mean free path shorter than their own size), but it is valid throughout a large part of the solar nebula including the formation region of the Earth. A basic assumption of this model is that aggregates do not restructure, i.e. that any contact made between grains stays forever and cannot be moved. Physically, this is equivalent to the assumption that collision energies are much lower than the energy required to initiate restructuring. This energy is given by the rolling energy

$$E_{\text{roll}} = 6\pi^2 \gamma R \xi_{\text{crit}}. \quad (2)$$

In Eq. (2), γ is the surface energy, R is the reduced radius of two monomers in contact, and ξ_{crit} is the critical displacement needed to initiate irreversible rolling. We refer the reader to Dominik & Tielens (1997); Chokshi et al. (1993) for detailed description of the contact physics.

In Paszun & Dominik (2006) this model has been used to collide aggregates of equal size and is capable to simulate small aggregates, which was sufficient for the comparison with zero-gravity laboratory experiments (Krause & Blum 2004). To study the effects of hierarchical growth, aggregates must be built that consist of millions of monomers. To speed up the search for new contacts between colliding aggregates, we have implemented an efficient nearest neighbor search (NNS) algorithm to improve the performance of the model (Hockney & Eastwood 1988). The algorithm we are using is optimized for the special setup of the model: there is no need to search for nearest neighbors within each aggregate, but only between grains of different aggregates. Therefore, we keep the particle lists for each aggregate separate. With the nearest neighbor search, the dependence of the computation time on the number of monomers is now reduced from $\mathcal{O}(N_1 \times N_2)$ to $\mathcal{O}(N_2 \times \log(N_1))$.

The computations are very efficient and allow the construction of aggregates with up to 10^7 monomers. The computational bottleneck is no longer the collision search, but the rotation of the large target aggregate which requires N matrix operations to compute positions of the monomers for each time step. However, it turns out that we can safely

ignore rotation for the present study, because the rotation of the large aggregate will quickly become negligible. In order to demonstrate this, let's assume that the kinetic energy E governing the random motions of the aggregates (for example through Brownian motion) remains constant during the growth. As the mass of the projectiles remains constant during the hierarchical growth process, we keep the approach velocity of a small projectile v_p constant as well. As the target becomes larger, its own random motions can be ignored and the approach velocity is dominated by the velocity of the small projectile. In order to see if the rotation of the target is important, we need to compare the linear approach velocity with the velocity of the outer regions of the target caused by its rotation. The angular velocity of a target particle is given as

$$\omega_t = \sqrt{\frac{2E}{I}} = \sqrt{\frac{2E}{Cm_0NR^2}}, \quad (3)$$

where I is the moment of inertia, m_0 is a monomer mass, and the constant C depends on a geometry of an aggregate (e.g. for a sphere $C = 2/5$). The equivalent circumferential speed is then

$$v_{\text{cir},t} \propto \sqrt{\frac{1}{N}} \quad (4)$$

and decreases with increasing mass. Even if the approach velocity is comparable to the velocity caused by rotation initially, when target and projectile are of similar size, the ratio of the two velocities quickly approaches zero as the target is growing. Therefore, we will conduct most of this study ignoring rotation during approach. We will, however, confirm the validity of this assumption with a test calculation (see Sect. 4.3). Within a few collision timescales the rotation of the target aggregate effectively stops and only rotation of projectiles can be considered. We will discuss this effect separately in Sect. 4.

A schematic picture of a collision configuration is shown in Fig. 1. A target aggregate initially is of the same size

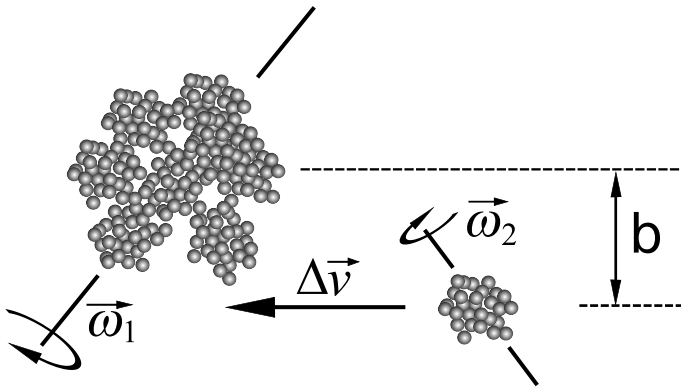


Fig. 1. A sketch of a collision. Aggregates rotate around a random axis and approach at random impact parameter b . The relative velocity Δv is assumed to be in the hit-and-stick regime.

as the incoming projectile. As the growth progresses, the size of the target increases. Thus the process starts as a perfect case of the CCA aggregation and smoothly turns into the PCA-like hierarchical case. In the cases where we do treat rotation, both particles spin around random axes with rotation velocities ω_i . All velocities are drawn from

the Maxwell distribution. The temperature is assumed to be 300 K and monomers are 1 micron (in diameter) sized silica spheres.

To quantify the structure of aggregates produced by hierarchical growth, we use the filling factor within a sphere enclosing the entire aggregate

$$\phi = N \left(\frac{r_0}{r_{\text{out}}} \right)^3, \quad (5)$$

where N is number of particles in an aggregate, r_0 is the monomer radius, and r_{out} is the outer radius of the aggregate.

PCA particles generally have a uniform density structure, meaning that the filling factor is constant throughout the core of an aggregate. The density will not be constant throughout the entire aggregate because of an inevitable transition region in the outer parts of the aggregate - we will discuss this region in more detail in Sect. 4.1. CCA aggregates, on the other hand, are known to have a fractal structure resulting in a density decreasing from the core to the outer regions with a power law dependence

$$\rho(r) \propto r^{D_f-3}, \quad (6)$$

where D_f is the fractal dimension and is about 1.5 for the ideal CCA process (Krause & Blum 2004; Paszun & Dominik 2006).

To study the effects of projectile size, we grow aggregates by sequential addition of particles of constant mass. We sample over two orders of magnitude in projectile mass. Our smallest projectiles are monomers, and the largest are built of 256 grains. The intermediate masses are successive powers of two in monomer mass ($2^0 m_0, 2^2 m_0, \dots, 2^8 m_0$).

It is to be expected that the internal structure of the projectiles will also have influence on the resulting aggregates. We cover this parameter by considering two extreme cases for growing the projectiles. In the first case, projectiles are made by PCA aggregation, leading to projectiles with an upper limit (reached only in the case of large aggregates) for the filling factor of $\phi = 0.15$ (Kozasa et al. 1992). The real aggregates used for this simulations have lower filling factors, typically $\phi \approx 0.05$.

3. Results

We present the internal structure of 16 aggregates produced in the hierarchical growth using projectiles of different structure and mass. Table 1 shows the final size of the grown aggregates in units of the projectile mass. Note that in terms of number of monomers, the largest aggregates are the ones made of large projectiles, reaching about 6.5×10^6 monomers for the aggregates grown from 256-mers. However, we give the mass in units of the projectile mass because the degree to which the structural limit of hierarchical growth can be reached is determined by this number rather than the number of monomers. The growth of largest particles is limited to 25000 projectiles.

3.1. Non-fractal (PCA) projectiles

The simplest case of the hierarchical growth is the sequential addition of monomers onto a larger target (the pure PCA case). This process has been studied before and we

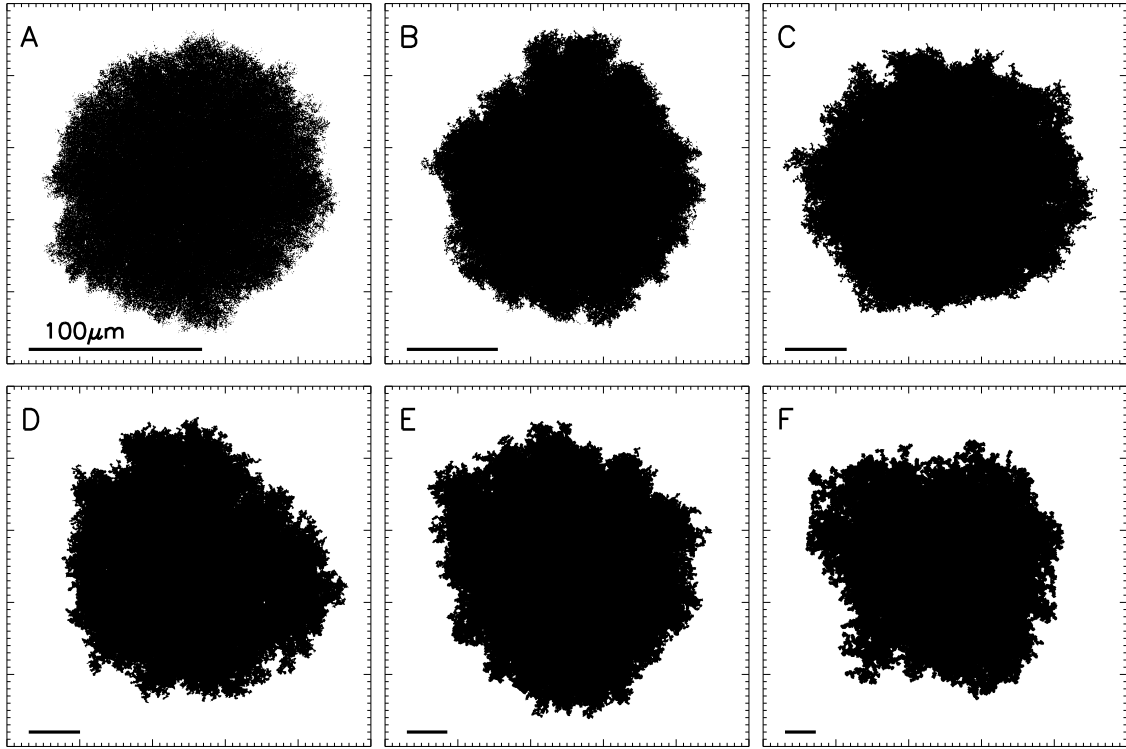


Fig. 2. Aggregates produced by a sequential coagulation of small PCA projectiles of a constant size. Each panel presents a horizontal bar indicating length of 100 μm . Projectile mass is: A- $N_p = 2^0$, B- $N_p = 2^2$, C- $N_p = 2^4$, D- $N_p = 2^5$, E- $N_p = 2^6$, F- $N_p = 2^8$.

Table 1. Mass of aggregates presented in this paper normalized to projectile mass. ^a - Simulation of hierarchical growth with rotation taken into account.

N_p	final N/N_p		
	aggregates made of bullet type PCA	CCA	CCA ^a
2^0	497 500	497 500	40 300
2^1	328 500	328 500	11 400
2^2	296 250	198 900	6 080
2^3	210 000	125 000	3 840
2^4	140 625	112 150	1 880
2^5	87 500	60 290	1 090
2^6	81 500	42 000	750
2^7	45 625	—	460
2^8	25 900	26 500	245

present it as a reference case in this study. Aggregates produced from PCA projectiles of different mass are presented in Fig. 2. The reference particle is shown in Fig. 2a. Its physical size is indicated by a scale bar that represents the length of 100 μm , i.e. 100 monomer diameters. This particle consists of approximately $N \approx 5 \cdot 10^5$ monomers (cf. Tab. 1). The remaining aggregates shown in the figure are grown from projectiles of increasing mass. They contain more monomers, but the number of impactors forming these aggregates decreases with increasing projectile mass. The largest aggregate consists of over $N = 6 \cdot 10^6$ monomers (Fig. 2f), but merely ~ 26000 projectiles (each consisting of 256 grains).

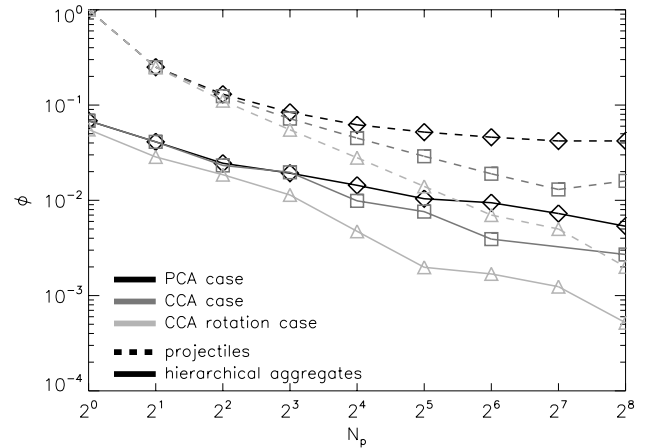


Fig. 3. The filling factor of aggregates formed by the hierarchical growth as a function of projectile size. The solid lines represent filling factor of final aggregates, while the dashed lines show the filling factor of projectiles. Black lines correspond to PCA case, while the grey lines to the CCA case.

The mass difference between the largest (Fig. 2f) and the smallest (Fig. 2a) aggregates is about one order of magnitude. The physical size also differs about one order of magnitude, which already indicates that the internal structure of agglomerates produced by the hierarchical growth depends on projectile size. This can directly be seen by inspecting the outer layers of all particles, where the size of voids increases with increasing projectile size (cf. Fig. 2a

– Fig. 2f). Also the overall filling factor decreases as the projectile size increases. This behavior is shown quantitatively in Fig. 3, along with the filling factors of the projectiles themselves. The filling factor of the PCA projectiles decreases from one (for monomers) to about 0.04 (for 256-mers) and clearly stabilizes at about this value. The filling factor of the aggregates formed by hierarchical growth (solid black line) decreases by over an order of magnitude as the PCA projectile mass increases from 1 to 256 monomers. Moreover, the decrease of the overall filling factor does not slow down as in the case of projectiles. This decrease for large, hierarchically grown aggregates is caused by two effects. The main effect is due to the decreasing filling factor of the projectiles. Since they can be considered as porous grains, their coagulation directly leads to a lower filling factor than in the pure monomer PCA case. However, as the filling factor of the projectiles is stabilizing near 0.04, one might expect that also the filling factor of the aggregates grown from these particles should stabilize, a result that is not evident in Fig. 3. As we will see below, this is caused by the comparatively large transition region close to the surface of the aggregate. For the largest projectiles, the computation has not advanced far enough to make the aggregate core dominate the overall filling factor. For a better view on the internal structure, we show in Fig. 4 the packing density $\phi(r)$ as a function of distance from the center of mass of an aggregate. The filling factor is roughly constant throughout

value $\phi = 0.0225 = 0.15^2$. This latter value would be expected from an idealized two-step aggregation process. The formation of the projectiles from monomers through PCA growth causes a filling factor of 0.15. If we assume that these aggregates are spherical as well, the following build-up of the target from these projectile aggregates lowers the filling factor by the same factor again. What is interesting here is that the filling factors of our projectiles were actually lower (0.04), due to the fluffy transition area at the projectile surface. From the simple argument above, we would expect a filling factor of $\phi = 0.04 * 0.15 = 0.006$. The fact that the true value is much closer to 0.15^2 shows that, apparently, the second growth step does compensate the low projectile filling factor by a certain degree of geometrical penetration. Since projectiles have fluffy surface regions, the first contact occurs after the projectile has penetrated a bit into the surface region of the target, filling some of the voids created by the projectile formation. This result is further discussed in Sect. 4.2.

The uniform density throughout the core of aggregates indicates that their structure is non-fractal. To verify this, we determine the fractal dimension D_f of our aggregates by fitting the data with a power-law function

$$N(r_g) = K \left(\frac{r_g}{r_0} \right)^{D_f}, \quad (7)$$

where K is the fractal pre-factor and r_g is the radius of gyration defined as

$$r_g = \sqrt{\frac{\sum_i^N r_i^2}{N}}, \quad (8)$$

with r_i being a distance of i -th grain from the center of mass. This gyration radius is calculated for an aggregate at different stages of its growth sequence. Since the structure of the projectiles influences the fit at small $N(r_g)$, the power-law exponent D_f is fitted to the outer half of the mass of an aggregate. The resulting fractal dimensions of different particles are shown in an inset of Fig. 4. The fractal dimension oscillates between $D_f = 2.9$ and $D_f = 3.0$, which shows the non-fractal structure of particles, as expected for the PCA case (Ball & Witten 1984).

3.2. Fractal (CCA) projectiles

CCA growth produces porous, fractal aggregates (Krause & Blum 2004; Paszun & Dominik 2006). The filling factor of these particles depends on mass (due to fractal structure) and is lower than that of PCA clusters of equal mass. This is a direct result of the CCA process, in which the void volume is increased with every growth step. The hierarchical growth with these fluffy projectiles is expected to produce more porous particles than in the case of PCA bullets.

The Results of hierarchical growth by a sequential agglomeration of CCA particles are presented in Fig. 5. At first sight, in comparison with the PCA bullet case, these aggregates show no spectacular differences. All particles have an approximately spherical shape and indicate an increase of porosity with increasing bullet mass. In Fig. 5a we present the *reference* aggregate made by a sequential accumulation of monomers. Note that this is just a copy of the aggregate in Fig. 2a. Even though the total mass of aggregates made of fractal (CCA) bullets is lower (cf. Tab. 1),

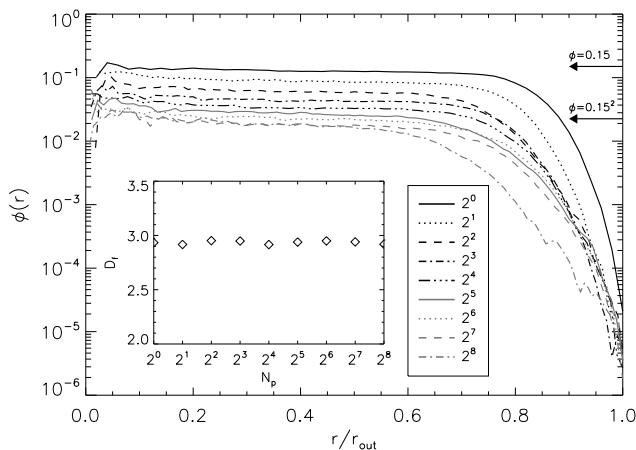


Fig. 4. Density structure of aggregates formed by a sequential incorporation of small PCA bullets. Different lines correspond to aggregates formed out of projectiles of different masses. From top to bottom, projectile masses are: $N_p = 2^0, 2^1, 2^2, \dots, 2^8$. The inset shows the fractal dimension D_f determined for these aggregates as a function of the mass of a projectile.

the inner region of aggregates. Small fluctuations indicate local inhomogeneities due to the finite size of monomers. These local density variations increase with increasing projectile mass, an effect of the larger building units and their own internal structure. The core density structure of two aggregates made of the largest projectiles ($N_p = 128$ and $N_p = 256$) is very similar. In combination with the result that the projectile filling factors were very similar, this indicates that the resulting density of an aggregate formed by hierarchical growth is mainly a function of the filling factor of the building components. In fact, filling factor in the inner region has the value of about $\phi \approx 0.02$, not far from the

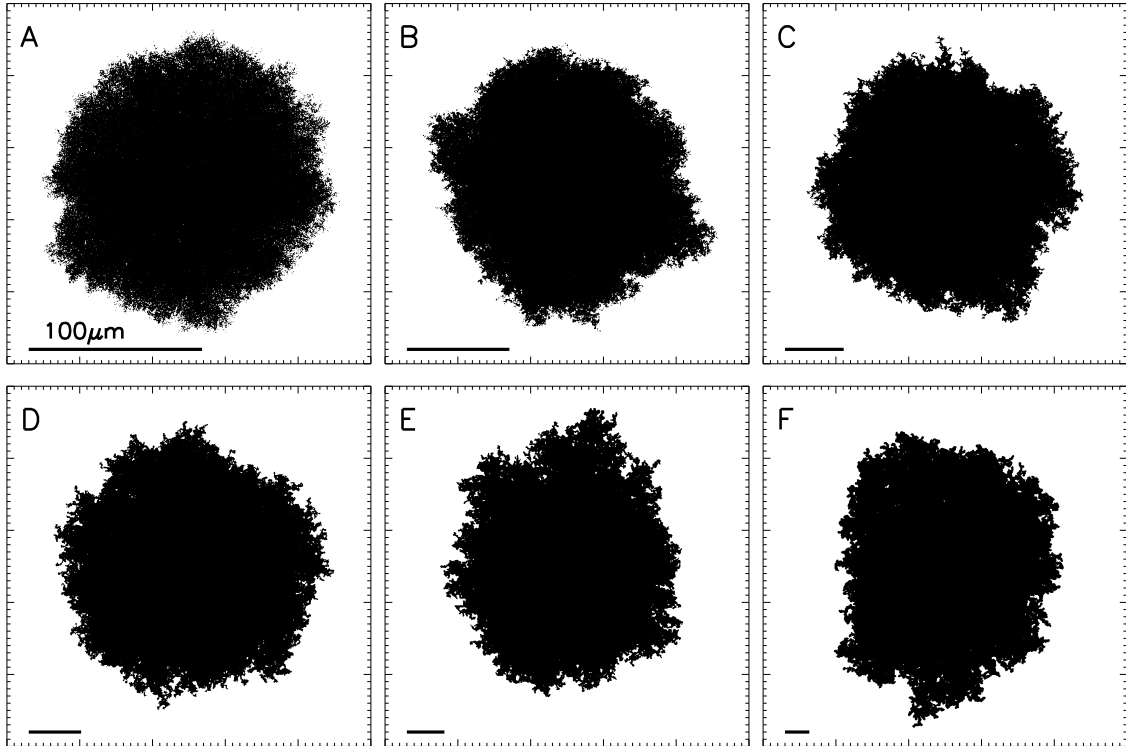


Fig. 5. Aggregates produced by a sequential coagulation of small CCA projectiles of a constant size. Each panel presents a horizontal bar indicating a length of $100 \mu\text{m}$. Projectile mass is: A- $N_p = 2^0$, B- $N_p = 2^2$, C- $N_p = 2^4$, D- $N_p = 2^5$, E- $N_p = 2^6$, F- $N_p = 2^8$.

the size (as indicated by the bar in each panel of Fig. 5) is very similar to or even larger than in the case of PCA projectiles. Obviously, the global filling factor of the new aggregates is much lower now. Quantitatively this is shown in Figure 3. The solid, grey line indicates the filling factor of aggregates produced by the hierarchical growth with CCA projectiles. For monomer and dimer *bullets*, the agglomerates are obviously identical since the bullets are identical as well. However, even for quadrumer and octomer bullets, the filling factors of the final aggregates are identical both for CCA and PCA bullets. However, this is a direct consequence of the fact that the filling factors of bullets themselves hardly differ from each other at these small sizes. Starting at $N_p \geq 2^4$, the differences between the targets do become significant and again simply reflect the changes in the bullet properties.

Again, the filling factors plotted in Figure 3 are influenced by the fluffy transition region close to the aggregate surface. A better view at the limiting filling factors that are reached by this process and realized in the cores of the aggregates is given in Figure 6 which shows the density structure of aggregates made of different CCA projectiles. An increasing projectile size results in a decrease of the central filling factor. For large CCA projectiles ($N_p = 2^5 \dots 2^8$) the filling factor decreases below the values obtained in the case of PCA projectiles (cf. Fig. 4). The aggregate made of the largest *bullets* has a central filling factor $\phi = 10^{-2}$, about a factor 2 lower than the value obtained for the corresponding PCA projectiles, due to the lower filling factor of the CCA *bullets*. The more irregular structure of the CCA projectiles also causes the stronger “noise” in the filling factor in the

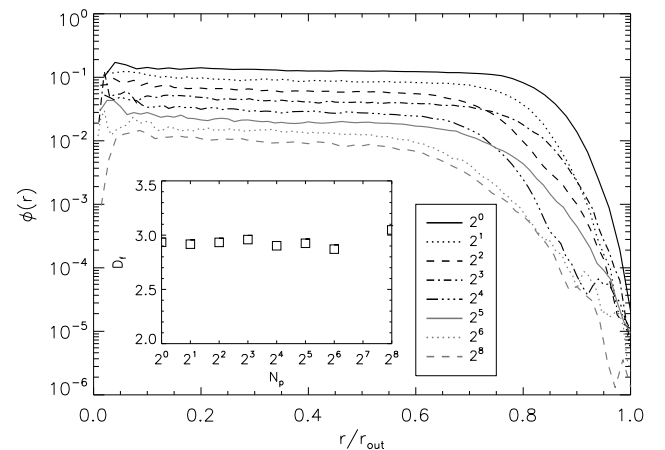


Fig. 6. Density structure of CCA aggregates formed without rotation. Different lines correspond to aggregates formed out of projectiles of different masses. From top to bottom, projectile masses are: $N_p = 2^0, 2^1, 2^2, \dots, 2^8$. The inset shows the fractal dimension D_f determined for these aggregates as a function of the mass of a projectile.

inner regions of aggregates at $r < 0.2r_{\text{out}}$. Even though the CCA projectiles are fractals, this property is lost in larger aggregates during the hierarchical growth. The filling factor in a final agglomerate is approximately constant throughout the inner half of the aggregate’s radius and declines only in the outer, porous layers. *Therefore the internal structure of hierarchical aggregates made of fractal projectiles is homo-*

geneous and non-fractal. The inset in Fig. 6 shows the fractal dimension of these aggregates. Clearly the initial fractal nature of projectiles diminishes, as the fractal dimension determined for these hierarchical aggregates is very close to $D_f = 3.0$.

4. Discussion

We have shown that hierarchical growth in the pure form which we have studied here produces aggregates whose structure depends mostly on the filling factor of the projectiles. However several other effects may also play a role. Here we address the influence of these additional factors. The influence of the fractal surface region is addressed in Sect. 4.1. The importance of aggregate penetration (tooth-ing) on the filling factor of the resulting aggregates is discussed in Sect. 4.2. The effect of rotation is presented in Sect. 4.3 and illustrated with additional simulations. Finally the relevance of the hierarchical growth for coagulation of dust in protoplanetary disks is discussed in Sect. 4.4.

4.1. Surface porosity

PCA aggregates show a dependence of the global filling factor on the aggregate mass. The reason for this is that the filling factor is affected by the fluffy, outer layers. This *transition region* initially covers the entire particle. As growth proceeds, projectiles are filling voids and build the constant-density core of an aggregate with the filling factor $\phi = 0.15\phi_p$. Eventually, the density in the center of an aggregate is high enough to prevent projectiles from entering. In the mean time, however, the aggregate has grown and a new transition region has appeared near the surface.

We determine the influence of these outer layers on the global filling factor as a function of aggregate mass. To approach the limit of $\phi = 0.15$ for the pure PCA growth, the effect of the transition region must decrease with an increasing aggregate size. Figure 7 shows the density structure of a single PCA aggregate obtained at different growth stages. To determine the thickness of the transition layer r_{tr} , we fitted an arbitrary function $f(r) = 1/r + \phi_0$, with the fitting parameter ϕ_0 , to the inner (core) region of an aggregate at different stages. As the beginning of the transition layer we assume a radius of an aggregate, where the filling factor drops below the fitted function by $\Delta\phi = 0.01$ ($\sim 10\%$).

Accumulation of monomers causes an increase of the outer radius r_{out} but also causes an increase of the thickness of the outer porous layer r_{tr} . However, the increase of the transition layer is slower than the increase of the aggregate size. This behavior is shown in the inset of Fig. 7. Indicated error-bars are estimated by changing the criterion for the onset of the transition regime by 10%. The thickness of the transition region relative to the outer radius of an aggregate decreases as the growth proceeds. Moreover we can show that the volume of the transition region is decreasing. This transition region corresponds to a volume of

$$V_{tr} = \frac{4}{3}\pi(r_{out}^3 - r_{tr}^3), \quad (9)$$

and when we divide Eq. (9) by the total volume $V = 4/3\pi r_{out}^3$, we find

$$\frac{V_{tr}}{V} = 3 \frac{r_{tr}}{r_{out}} - 3 \left(\frac{r_{tr}}{r_{out}} \right)^2 + \left(\frac{r_{tr}}{r_{out}} \right)^3. \quad (10)$$

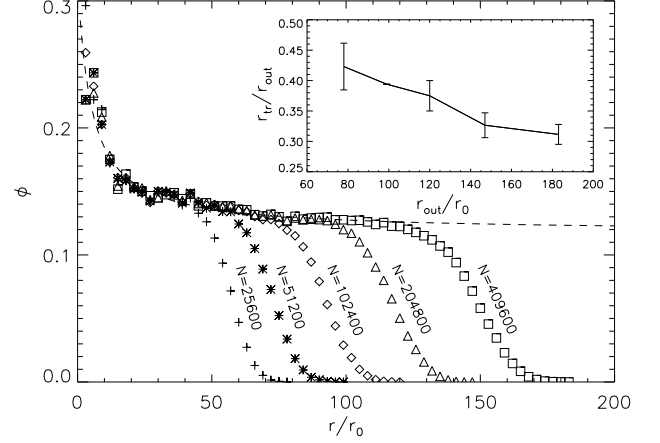


Fig. 7. The filling factor as a function of aggregate size. The growth sequence is shown at 5 different stages: $N = 25600$, $N = 51200$, $N = 102400$, $N = 204800$, $N = 409600$ monomers. The dashed line shows a fit to the data of the inner part of the aggregate at the most advanced growth stage. The transition layer is defined here as the region, where the filling factor is lower than the fit by more than 10%. The inset shows the relative size of the transition layer as a function of aggregate size. Again 5 different growth stages are indicated.

Thus the volume ratio decreases with a decreasing ratio of r_{tr}/r_{out} . Therefore the influence of the outer, fluffy layers weakens with increasing size. In the limiting case, this outer, fluffy region is relatively very thin leading to a filling factor of about $\phi = 0.15$.

4.2. The core porosity and the toothing radius

The core density of hierarchical aggregates shows that their filling factor results from PCA-like growth of porous particles. Therefore, the packing density is chiefly the product of the PCA filling factor ($\phi = 0.15$) and the filling factor of a projectile. In the case of PCA bullets the filling factor reaches the value of $\phi \approx 0.02$ (cf. Fig. 4), indicating penetration of projectiles into the target (see Sect. 3.1). The lower the filling factor of the projectile, the larger the surface voids in the particles are, and the larger the overlap is expected to be. Figure 8a shows the ratio of aggregate over projectile filling factor for aggregates formed from different projectiles. The deviation from the $\phi/\phi_p = 0.15$ line is evidently increasing with decreasing filling factor. The exception of PCA particles results from the non-fractal structure of these projectiles. Their low filling factor ϕ is caused by the extended, outer transition region. Therefore, a further increase in size of projectiles results in an increase of the filling factor of PCA projectiles (because the relative thickness of the transition region decreases, as shown in Sect. 4.1) and eventually reaches the limit of $\phi/\phi_p = 0.15$ at $\phi_p = 0.15$. CCA projectiles on the other hand have a fractal nature and thus their filling factor decreases with increasing size. This results in a continuous increase of the ratio of the aggregate to the projectile filling factor, as the intersection is increasingly larger. Therefore the filling factor of a final aggregate can be presented as the PCA growth, where the final filling factor is given by $\phi = 0.15\phi_p$ and a correction due to the penetration and the resulting increase of the

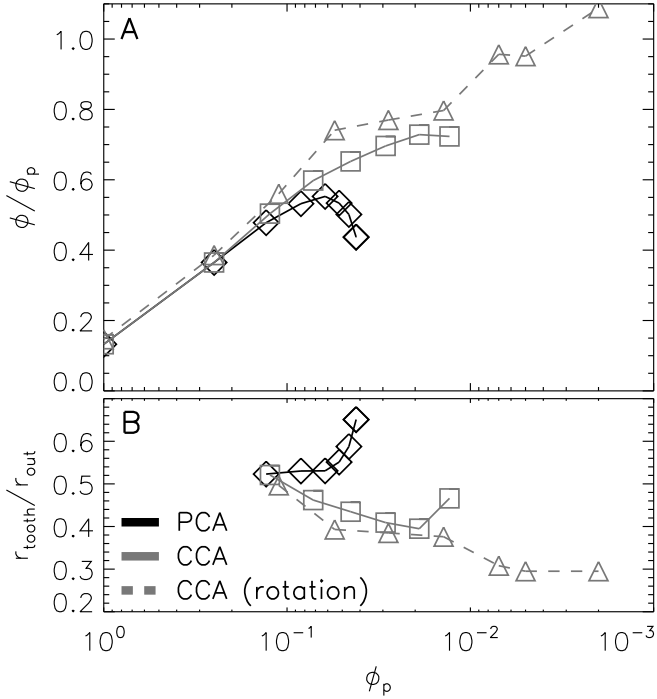


Fig. 8. A - The core filling factor of hierarchically grown aggregates normalized to the filling factor of projectiles. The core filling factor is determined by taking the filling factor of the inner part of an aggregate only. In this case we determined the packing density within a sphere with a radius of half of the outer radius. The dotted line indicate a relation fitted to the data. B - a tooting radius r_{tooth} of projectiles. See text for further explanation.

actual density. The correction must be a function of the projectile porosity, as more fluffy aggregates can be penetrate deeper. Following this path we fitted a simple function to our data

$$\phi = 0.15 \phi_p - \zeta \phi_p \log \phi_p, \quad (11)$$

where $\zeta = 0.368 \pm 0.012$ is a constant obtained from the least square fit.

The penetration depth can be expressed in terms of a tooting radius r_{tooth} . This quantity has been introduced by Ossenkopf (1993) as “half of the distance of the centers of two equal size clusters that are on average sticking to each other”. Thus in our case the tooting radius r_{tooth} is given by

$$\frac{\phi}{\phi_p(r_{\text{tooth}})} = 0.15, \quad (12)$$

where

$$\phi_p(r_{\text{tooth}}) = N_p(r_{\text{tooth}}) \left(\frac{r_0}{r_{\text{tooth}}} \right)^3 \quad (13)$$

is the filling factor of a projectile determined at $r = r_{\text{tooth}}$. Therefore a low tooting radius means that the penetration is deep and aggregates overlap significantly. Figure 8b shows the tooting radii obtained for projectiles with different filling factors. PCA particles are characterized by rather large tooting radii, meaning that the penetration must be relatively shallow. Intuitively, the tooting radius

of non-fractal aggregates should approach the outer radius in the limit of large agglomerates (i.e. for PCA projectiles $\lim_{n \rightarrow \infty} \frac{r_{\text{tooth}}}{r_{\text{out}}} = 1$). Here PCA particles still suffer from the extended, porous, outer transition region. Thus the average penetration depth is relatively deep ($r_{\text{tooth}}/r_{\text{out}} < 0.65$ for $N_p \geq 2^7$). Figure 8b shows, however, that the tooting radius increases very steeply for PCA particles. It may thus be expected that for larger sizes (and filling factor $\phi = 0.15$) the tooting radius will approach the outer radius.

Fractal projectiles on the other hand show very different behavior. In this case the penetration depth increases with the increasing size up to 70% of their outer radius for largest aggregates ($N_p = 2^8$). Aggregates of different fractal dimension (CCA particles formed in the presence of rotation are characterized by $D_f \approx 1.5$, while these formed without rotation have $D_f \approx 2.0$) seem to behave in a similar way indicating that the main parameter is the filling factor of the projectile, not the precise structure. We note that the final increase of the relative tooting radius for CCA aggregates in Fig. 8b and flattening in Fig. 8a are probably caused by chance effects due to the random aggregate shape and the limited size of the final aggregates (see section 4.3).

4.3. The influence of rotation

We have shown in Sect. 2 that, as long as rotation and linear motion are associated with similar energies, the effect of rotation on hierarchical growth should be small. However, the formation of small CCA projectiles is in fact influenced significantly by rotation, and we expect that hierarchical growth will reflect the increased projectile porosity.

Even though the size of aggregates produced in simulations treating aggregate rotation is limited, we show the effect of including rotation with an example calculation. The overall filling factor of aggregates formed with rotation is shown, along with the filling factors discussed earlier, in Fig. 3. Even for the smallest projectiles (monomers and dimers are structurally identical to the non-rotation case), there is a weak decrease in filling factor. This is the direct, limited influence of projectile rotation during the collision. The shift in filling factor seems to be approximately constant for the small projectiles. However, starting with 8-mers, the effect is clearly visible, both in the filling factor of the projectile, and consequentially in the filling factor of the produced large aggregate. The difference of the filling factor between growth using monomers and using 256-mers reaches two orders of magnitude. Going back to figure 8, it is interesting to see that the ratio of final to projectile filling factor follows the same trend already established for the non-rotation simulations. This re-enforces our notion that for hierarchical growth, rotation can be neglected when building up the large aggregate from smaller ones, but it cannot be ignored when constructing the projectiles.

Figure 9 shows the density structure of several aggregates made of different masses of CCA projectiles formed in the presence of rotation. Particles made of largest projectiles contain only a few hundred bullets and thus have not yet fully converged to the final structure. Even close to the core the density will still increase somewhat. Although the density of some aggregates is not homogeneous throughout the inner regions, the fractal dimension determined for all aggregates indicates non-fractal structure, as presented

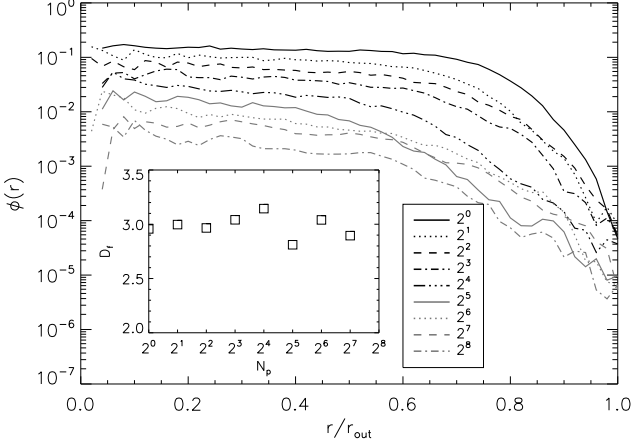


Fig. 9. Density structure of CCA aggregates formed with rotation. Different lines corresponds to aggregates formed out of projectiles of different masses. From top to bottom projectile masses are: $N_p = 2^0, 2^1, 2^2, \dots, 2^8$. The inset shows the fractal dimension D_f determined for these aggregates as a function of the mass of a projectile.

in the inset of Fig. 9. The fractal dimension is scattered around $D_f = 3.0$ and does not fall below $D_f = 2.7$.

4.4. Relevance of the hierarchical growth.

Hierarchical growth produces aggregates of very porous and non-fractal structure. This affects both the collision cross-section and the strength of particles as the packing density determines the ability to restructure or erode an aggregate (Paszun & Dominik 2008). Since the influence of the outer fluffy layers of agglomerates on the average filling factor depends on mass (cf. Sect. 4.1), it is important to understand conditions under which hierarchical growth takes place. For this purpose we employ a simple model of the minimum-mass solar nebula (Hayashi 1981) to obtain quantities that characterize the gas component (Table 2; after Takeuchi & Lin (2002) and Ormel et al. (2008a)). We assume a turbulent state of the gas with the strength parameter $\alpha = 10^{-2}$. The turbulent viscosity is given by (Shakura & Syunyaev 1973)

$$\nu_T = \alpha c_s H_g = \alpha c_s^2 \Omega^{-1}, \quad (14)$$

with H_g being the scale height of the gas disk and Ω being the local Kepler frequency. The overturn time of the smallest eddy is

$$\tau_s = \text{Re}^{-1/2} \tau_L, \quad (15)$$

with the Reynolds number $\text{Re} = \nu_T / \nu_m$, where $\nu_m = c_s \lambda / 2$ is the molecular viscosity (Cuzzi et al. 1993). Here we consider only two main sources of relative velocities between dust particles:

1. *Thermal (Brownian) motions.* Dust particles collide with gas molecules resulting in transfer of the momentum. These collisions give a push from random directions causing Brownian motion of dust particles. Relative velocities between two aggregates of mass m_1 and m_2 are then given by

$$\Delta v_{\text{BM}} = \sqrt{\frac{8\pi k_B T (m_1 + m_2)}{\pi m_1 m_2}}, \quad (16)$$

where k_B is Boltzmann's constant. These relative velocities are very low ($\sim \text{mm/s}$ for micron-sized particles) and decrease further for larger sizes.

2. *Turbulence.* Dust aggregates respond to the gas on a timescale given by the stopping time τ_f (see Eq. (1)). The mean turbulent gas velocity fluctuations $v_g = (3/2)^{1/2} \alpha^{1/2} c_s$ (Cuzzi & Hogan 2003; Ormel et al. 2008a) are not immediately mirrored by dust particles, resulting in relative motions between dust particles as particles of different stopping time have different velocities. These relative velocities are given in a simple form (Voelk et al. 1980) as $\Delta v_{12}^2 = \Delta v_{\text{II}}^2 + \Delta v_{\text{I}}^2$ where subscripts II and I denote contributions due to fast (class II) and slow (class I) eddies. The two terms are given as a function of the Stokes number of the particles by (for a complete derivation see Ormel & Cuzzi 2007)

$$\Delta v_{\text{I}}^2 = v_g^2 \frac{\text{St}_1 - \text{St}_2}{\text{St}_1 + \text{St}_2} \left(\frac{\text{St}_1^2}{\text{St}_{12}^* + \text{St}_1} - \frac{\text{St}_1^2}{1 + \text{St}_1} - (1 \leftrightarrow 2) \right) \quad (17a)$$

$$\Delta v_{\text{II}}^2 = v_g^2 \left((\text{St}_{12}^* - \text{Re}^{-1/2}) + \frac{\text{St}_1^2}{\text{St}_1 + \text{St}_{12}^*} - \frac{\text{St}_1^2}{\text{St}_1 + \text{Re}^{-1/2}} + (1 \leftrightarrow 2) \right). \quad (17b)$$

Here the term St_{12}^* is obtained by solving eq.21d from Ormel & Cuzzi (2007) and is given by $\text{St}_{12}^* \approx 1.6 \frac{\max(\tau_1, \tau_2)}{\tau_L}$ for small particles ($\tau_L \gg \tau_f$), and $\text{St}_{12}^* \approx \frac{\max(\tau_1, \tau_2)}{\tau_L}$ for $\tau_f \approx \tau_L$.

We use these velocities to determine under what circumstances hierarchical growth is relevant. First we discuss which particles of a given size distribution contribute most to the growth of a larger aggregate. Then we also consider typical impact energies to infer if and for what particles our idealized hit-and-stick assumptions are applicable.

4.4.1. Small particle contributions to growth

In Sect. 1 we have already motivated that hierarchical growth needs to be considered in a situation where on-going fragmentation leads to a replenishment of small particles. To investigate the mass contribution of different size aggregates to the growth, we will assume a *flat* mass spectrum of dust particles, i.e. a distribution that is given by $f(m)m^2 d \log m = \text{const}$. In this case, the mass in a logarithmic interval between $\log m$ and $\log m + d \log m$ is constant. This assumption is a reasonable approximation to the results of numerical simulations including fragmentation (e.g., Brauer et al. 2008; Ormel et al. 2008b). The mass accumulation rate of a target aggregate is then given by

$$\frac{dm_t}{dt} = \int_{m_1}^{m_2} f_p(m) m_p^2 \sigma_{\text{coll}} \Delta v dm, \quad (18)$$

where $f_p(m)$ is density of projectiles of mass N_p and $\sigma_{\text{coll}} = \pi(r_p + r_t)^2$ is the cross-section for collision between target aggregate and a projectile. Figure 10 shows the *cumulative* mass accumulation rate \dot{m}_t for every target aggregate.

Table 2. Gas parameters corresponding to a minimum-mass solar nebula model with total mass of $2.5 \cdot 10^{-2} M_{\odot}$ within 100AU. The radial distribution of the surface density and the temperature have a power-law form with slope of -1 and -0.5 , respectively.

parameter	symbol	adopted value	units
Gas density	ρ_g	28./0.16	$10^{-11} \text{ g cm}^{-3}$
Sound speed	c_s	10./5.6	10^4 cm s^{-1}
Mean free path (gas)	λ	6.9/1230.	cm
Temperature	T	280./89.	K
Large eddy overturn time	$\tau_L = \Omega^{-1}$	0.16/5.0	yr
Turbulence strength parameter	α	10^{-2}	
Smallest eddy turnover time	τ_s	1.3/131	10^3 s

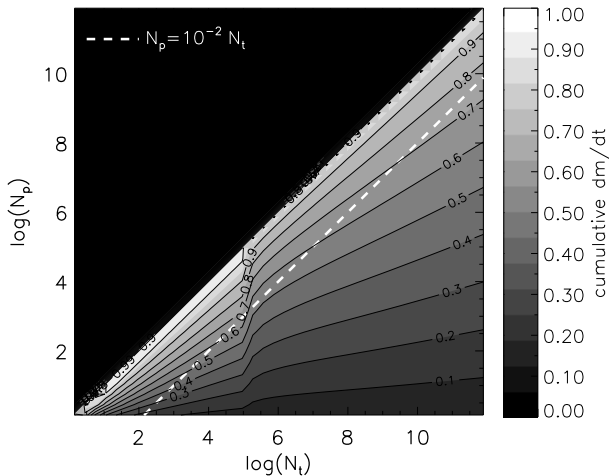


Fig. 10. Cumulative mass accumulation rate for PCA aggregates. The mass gain is normalized such that the total accumulation is unity for all projectiles smaller or equal to the target mass. The dashed line indicates the projectile size that has two orders of magnitude smaller mass than the target ($N_p = 10^{-2} N_t$). The change in the mass accumulation rate at about $N_t \approx 10^5$ indicates a change in relative velocities due to decoupling of aggregates from the smallest eddies.

For each target (N_t) and projectile (N_p) we show the mass contribution from all projectiles smaller or equal to N_p .

Given these assumptions, Figure 10 clearly shows that for all but the smallest aggregates, the growth is dominated by projectiles much smaller than the target. The dashed line indicates a projectile mass two orders of magnitude smaller than the corresponding target particle. Therefore aggregates made of more than $\sim 10^5$ monomers collect over 60% of the total coagulated material from particles of masses smaller than 0.01 of their own. This indicates a great importance of hierarchical growth, as the coagulation is dominated by collisions with significantly smaller particles.

Prediction of the aggregate structure that results from the hierarchical growth, requires a coagulation model that follows the evolution of both the mass and the filling factor of dust aggregates. This issue is going to be the subject of a follow-up study.

4.4.2. Impact energy and the hit-and-stick approximation

As the hierarchical growth has a great importance in the coagulation of dust aggregates, we now need to focus on the energy available during a collision and verify under

what conditions this energy is consistent with the assumptions made in this paper. We have shown in Sect. 3.1 and Sect. 3.2 that the structure of aggregates in the hit-and-stick regime is determined almost entirely by the filling factor of projectiles. This opens up a very simple way to compute filling factors of aggregates in this regime. Higher collision energies will result in restructuring and thus affect the final porosity of aggregates (making them more compact). The restructuring threshold depends on both material properties and monomer size (cf. Eq. (2)). We keep these quantities as free parameters in the following derivation. The surface energy γ for two species we adopt is $\gamma_{\text{sil}} = 25 \text{ erg cm}^{-2}$ for silicate monomers and $\gamma_{\text{ice}} = 370 \text{ erg cm}^{-2}$ for ice coated silicate grains. In the latter case the mass of aggregates is set by the bulk density of silicates ($\rho_0 = 2.65 \text{ g cm}^{-3}$), while the restructuring is determined by the ice mantle. We also consider three different monomer sizes: $r_0 = 300$, $r_0 = 0.1 \mu\text{m}$, and $r_0 = 0.5 \mu\text{m}$.

Numerical simulations by Dominik & Tielens (1997) have shown that the first visible restructuring occurs above about five times the rolling energy (Eq. (2)). Later Blum & Wurm (2000) confirmed this finding in laboratory experiments. Therefore we take this energy threshold as the upper limit of the hit-and-stick regime. As for the relative velocities we continue with the minimum-mass solar nebula model adopted in Sect. 4.4.

We calculate the collision energies between different particles relative to the restructuring energy threshold: $E/(5 E_{\text{roll}})$. Note that the rolling energy E_{roll} scales for different materials (ice and silicates) with the surface energy γ only, as the critical displacement ξ_{crit} is assumed to be independent of material. Figure 11 shows the projectile mass for which the impact energy equals the threshold energy for restructuring. The different line styles indicate aggregates made of ice-coated monomers (dashed lines) and silicates grains (solid lines). Lines corresponding to different monomer sizes are labeled. Collisions occur between target aggregates (of mass N_t) and projectiles (N_p). For simplicity we assume a PCA structure of all aggregates, i.e. $\phi = 0.15$, which is really the worst case scenario. If more fluffy particles form due to hierarchical growth, the porosity will increase, changing the projected surface area of agglomerates. This affects both their collision cross-section and their stopping time. As a result, relative velocities will decrease, allowing hit-and-stick growth to proceed to even larger masses. Figure 11a shows the results at the distance of 1 AU from the central star. Aggregates made of about micron-sized silicate monomers ($r_0 = 0.5 \mu\text{m}$) can grow to about $N_t = 10^4$ grains, before any restructuring can occur. Smaller aggregates, of the order of $N_p \sim 10$ monomers, have impact energies above the threshold value when they col-

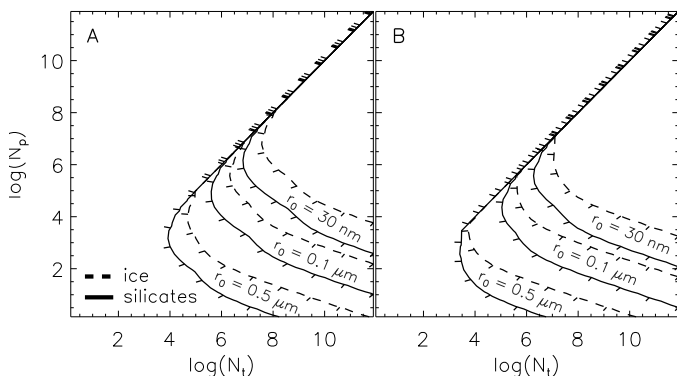


Fig. 11. The restructuring energy threshold ($E = 5E_{\text{roll}}$) for small monomers of $r_0 = 300$, $r_0 = 0.1$, and $r_0 = 0.5 \mu\text{m}$. The solid line correspond to silicate grains, while the dashed line corresponds to ice coated silicate grains. Short perpendicular ticks indicate a decrease direction of the collision energy. The two panels correspond to different distances from the central star in the minimum-mass solar nebula: A - 1AU and B - 10AU.

lide with very large targets made of over $N_t \sim 10^6$ grains. A significantly higher threshold velocity for smaller monomers allows for the hit-and-stick growth up to greatly larger aggregate sizes (in terms of the number of monomers). No restructuring occurs, regardless of the projectile mass, for target aggregates made of, respectively, up to over 10^6 and up to over 10^7 monomers for grain size of $0.1 \mu\text{m}$ and 300 . This effect is caused by both higher adhesion force per unit mass (increasing the rigidity of aggregates), and much shorter stopping times of aggregates made of smaller monomers (leading to smaller relative velocities). The effect of the difference in the rolling energy can be directly observed by comparing results for silicate grains with and without ice mantle. The higher surface energy of ice results in a threshold energy higher by about an order of magnitude (this is caused by the ratio of the surface energy of ice over that of silicates of $\gamma_{\text{ice}}/\gamma_{\text{sil}} = 14.8$) for the hit-and-stick growth.

Figure 11b shows the threshold energy for aggregates at 10 AU. In this case, lower densities (due to the negative radial density profile) result in longer stopping times of aggregates and thus higher relative velocities. The onset of restructuring at 10 AU, however, is only slightly different. The maximum number of monomers that can be reached without the onset of restructuring is only slightly smaller.

These results show that dust aggregates can grow several orders of magnitude in mass before any restructuring can occur. In the case of a weaker turbulence the relative velocities decrease. This results in the growth unaffected by restructuring to even larger sizes. For the parameter $\alpha = 10^{-4}$ particles will grow to masses about two orders of magnitude larger. The coagulation process in these conditions produces particles of very low filling factor, depending on the mechanism responsible for the growth of small projectiles.

Note that small aggregates can also collide with much larger particles (due to a flat mass spectrum) and cause restructuring. In such a case, however, these small aggregates are incorporated into bigger bodies (they are removed) and restructuring occurs only in this large particle. Moreover, very big particles (about $100 \mu\text{m}$ in size and larger) can bounce (Langkowski et al. 2007), which affects the structure

of both impactors if the impact energy is sufficiently high. This, however, requires growth to very big sizes, where restructuring is already involved in shaping the particle structure. Therefore, the hierarchical growth in this size regime must be considered together with a structural evolution due to collisional compaction (e.g., Paszun & Dominik 2008).

5. Conclusions

We have studied the process of hierarchical growth of dust aggregates, in which a large target aggregate is built up slowly by adding much smaller projectiles of constant size. We have shown that this process leads to aggregates that consist of a core and a surface transition region.

The core is non-fractal in nature, so it has a constant density. The density of this core results from the fact that it is built up in a PCA-like process from the projectiles. If the projectiles are particles that are relatively compact and spherical (i.e. PCA aggregates themselves), a good approximation for the final core density is the product of the volume filling factor of the projectiles ϕ_p times the PCA filling factor 0.15. For projectile aggregates that result from a CCA-like growth mechanism, the typical distance between projectile aggregates in the growing target is smaller than the circumscribing radius of the projectile, because the porous outer layers interpenetrate before the first physical contact. However, also in this case, we find that the final filling factor of the core is largely given by the filling factor of the projectiles and can be approximated very well by a simple relation (see Eq. (11)).

We also show that in a coagulation environment where relative velocities are driven by turbulence, a logarithmically flat mass distribution (equal mass per mass decade) immediately leads to a situation where small particles and aggregates dominate the growth of large ones. Therefore, in such environments, hierarchical growth should be seen as the norm. Consequently, we predict that the aggregates in such environments are not fractals with extremely low densities as they would result from extrapolation of fractal laws to large sizes. The compactification of aggregates does not only result from collisions with enough energy to restructure aggregates - it starts already earlier by filling voids in particles with smaller projectiles that contribute to the growth.

Acknowledgments

We thank Prof. Jürgen Blum for useful comments, Evghenii Gaburov for constructive discussions on the implementation of the nearest neighbor search algorithm, and Chris Ormel for input on the velocity field of particles in a disk model. We also thank SARA supercomputer center for providing us with access to computer cluster LISA, to run very time consuming simulations. Travel support of the Leids Kerkhoven-Bosscha Fonds has been important for this research, which was financed by the Nederlandse Organisatie voor Wetenschappelijk Onderzoek, Grant 614.000.309.

References

- Ball, R. C. & Witten, T. A. 1984, Phys. Rev. A, 29, 2966
- Bentley, M. S., Schmied, R., Mannel, T., et al. 2016, Nature, 537, 73
- Blum, J., Gundlach, B., Mühle, S., & Trigo-Rodriguez, J. M. 2014, Icarus, 235, 156

- Blum, J. & Wurm, G. 2000, *Icarus*, 143, 138
- Brauer, F., Dullemond, C. P., & Henning, T. 2008, *A& A*, 480, 859
- Brauer, F., Dullemond, C. P., Johansen, A., et al. 2007, *A& A*, 469, 1169
- Chokshi, A., Tielens, A. G. G. M., & Hollenbach, D. 1993, *ApJ*, 407, 806
- Cuzzi, J. N., Dobrovolskis, A. R., & Champney, J. M. 1993, *Icarus*, 106, 102
- Cuzzi, J. N. & Hogan, R. C. 2003, *Icarus*, 164, 127
- Dominik, C. & Dullemond, C. P. 2008, *A& A*, 491, 663
- Dominik, C. & Tielens, A. G. G. M. 1997, *ApJ*, 480, 647
- Dullemond, C. P. & Dominik, C. 2005, *A& A*, 434, 971
- Hayashi, C. 1981, *Progress of Theoretical Physics Supplement*, 70, 35
- Hockney, R. W. & Eastwood, J. W. 1988, *Computer simulation using particles* (Bristol: Hilger, 1988)
- Kempf, S., Pfalzner, S., & Henning, T. K. 1999, *Icarus*, 141, 388
- Kozasa, T., Blum, J., & Mukai, T. 1992, *A& A*, 263, 423
- Krause, M. & Blum, J. 2004, *Physical Review Letters*, 93, 021103
- Langkowski, D., Teiser, J., & Blum, J. 2007, *ArXiv e-prints*, 711 [0711.2148]
- Lorek, S., Gundlach, B., Lacerda, P., & Blum, J. 2016, *A& A*, 587, A128
- Ormel, C. W. & Cuzzi, J. N. 2007, *A& A*, 466, 413
- Ormel, C. W., Cuzzi, J. N., & Tielens, A. G. G. M. 2008a, *ApJ*, 679, 1588
- Ormel, C. W., Paszun, D., Dominik, C., & Tielens, A. G. G. M. 2008b, in prep.
- Ossenkopf, V. 1993, *A& A*, 280, 617
- Paszun, D. & Dominik, C. 2006, *Icarus*, 182, 274
- Paszun, D. & Dominik, C. 2008, *A& A* submitted
- Shakura, N. I. & Syunyaev, R. A. 1973, *A& A*, 24, 337
- Takeuchi, T. & Lin, D. N. C. 2002, *ApJ*, 581, 1344
- Voelk, H. J., Jones, F. C., Morfill, G. E., & Roeser, S. 1980, *A& A*, 85, 316
- Weidenschilling, S. J. 1977, *MNRAS*, 180, 57
- Weidenschilling, S. J. & Cuzzi, J. N. 1993, in *Protostars and Planets III*, ed. E. H. Levy & J. I. Lunine, 1031–1060